Research Article Vol. 30, No. 5 / 28 Feb 2022 / Optics Express 6519
Optics EXPRESS

# Modeling amplified arbitrary filtered heterodyne microwave photonic links

ERICA SÁNCHEZ,[1,*] DANIEL PÉREZ-LÓPEZ,[1] DIEGO PÉREZ-GALACHO,[1] TAN HUY-HO,[2] DAVID WESSEL,[2] AND JOSÉ CAPMANY[1]

[1] *Photonics Research Labs, iTEAM Research Institute, Universitat Politècnica de València, Spain*
[2] *Ottawa Wireless Competency Center, Huawei Technologies Canada, Co, Ltd, Ottawa, Canada*
[*] *ersango@iteam.upv.es*

**Abstract:** We report an end-to-end analytic model for the computation of the figures of nerit (FOMs) of arbitrarily filtered and amplified heterodyne coherent microwave photonics (MWP) links. It is useful for evaluating the performance of complex systems where the final stage is employed for up/down-converting the radio frequency (RF) signal. We apply the model to a specific case of complex system representing the front-haul segment in a 5G link between the central office and the base station. The model can be however applied to a wider range of cases combining fiber and photonic chip elements and thus is expected to provide a useful and fast tool to analyze them in the design stage.



## 1. Introduction

Emerging applications such as 5/6 G mobile communications, Internet of Things (IoT) and industry 4.0 call for MWP systems with increased complexity [1–3] to provide a smooth interface between optical fiber-based transport networks and wireless edge segments. Complex MWP can perform in-flight arbitrary optical signal processing tasks and this feature can be modelled by including an arbitrary passive filter transfer function H(ω) in the optical part of the link [4]. Several works [4–7] have reported the derivation of the fundamental figures of merit of these complex systems for direct and self-heterodyne detection. At the same time, as complexity grows and/or more distance is covered by MWP systems, losses increase requiring the incorporation of optical amplification to improve the link performance [8]. Recent papers [9,10] have reported analytical models for amplified arbitrary filtered MWP links under direct detection and for amplified self-heterodyne frequency converters respectively. In this last reference, full expressions for the gain, Noise Figure (NF), and dynamic ranges have been derived although in the absence of optical filtering.

Another class of MWP systems exploits the receiver stage to provide the desired RF frequency up-conversion prior to antenna radiation [11]. This is achieved by coherent heterodyne detection, where a local laser oscillator is combined with the link signal instead of using the same input laser subject to parallel modulation by the RF and the local oscillator as proposed by Bottenfield and co-workers [10]. Here, we report an end-to-end model for these systems under arbitrary passive filtering and amplification. The model provides the expressions for the main FOMs for the case of In-phase and Quadrature (IQ) modulation. A distinctive feature of this model as compared to others reported before [8–10] is that it accounts for the impact of an arbitrary large chain of amplifier plus filter sections. These sections do not need to be identical, furthermore, they can be individually different. Thus, it can be applied to systems ranging from very simple to very complex configurations by scaling the number of sections in the system.

The paper is organized as follows: Section 2 provides the details of the analytic model including the equations for the constituent blocks and the derivation of the linear and nonlinear signal

#450974 https://doi.org/10.1364/OE.450974
Journal © 2022 Received 12 Dec 2021; revised 2 Feb 2022; accepted 4 Feb 2022; published 14 Feb 2022

Optics EXPRESS

components at the system output and the different relevant noise sources. Section 3 builds upon the results derived in section 2 to provide the analytical expression for the system FOMs. In section 4, we discuss the applicability and features of the model and use it to an application example.

## 2. Analytical model

### 2.1. System under consideration

Figure 1 shows the layout of the system under consideration. As it can be appreciated, it is composed of five main blocks: An input CW laser, the I-Q modulator, the arbitrary filtered and amplified chain, the local oscillator and the balanced detection stage. We briefly describe each one of them in the following subsections.

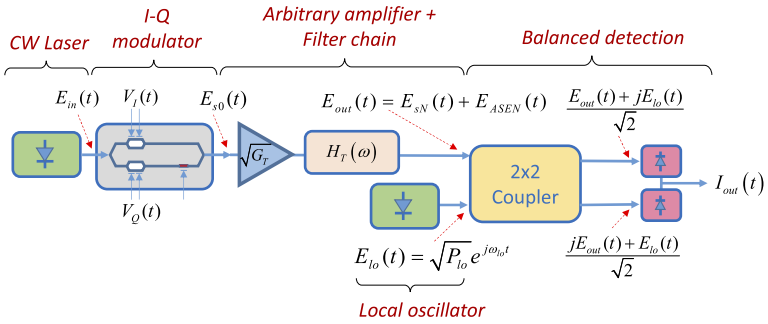


**Fig. 1.** Coherent heterodyne MWP system with arbitrary filtering and amplifying stages layout under consideration.

#### 2.1.1. CW laser

This provides the input optical field to the system, defined as:

$$E_{in}(t) = \sqrt{P_{in}}e^{(j\omega_0 t)} \tag{1}$$

where $P_{in}$ is optical power at the optical carrier frequency $\omega_0$ [4].

#### 2.1.2. I-Q modulator

Since we are dealing with a coherent detection system, we choose an I-Q modulator as an external device to modulate the RF information onto the laser intensity provided by the CW laser. By doing so, we can independently model the FOMs for each signal component. Note that we can always obtain particular FOM expressions for the single-drive Mach-Zehnder modulator case. The I-Q modulator electric field model corresponds to a dual parallel Mach-Zehnder modulator (DPMZM) shown in Fig. 2 and can be derived by suitable extension of the dual-drive MZM device presented in [4]:

Referring to Fig. 2 we consider the practical case where in-phase and quadrature dc bias values are equal $\phi_{dc,i} = \phi_{dc,q} = \phi_{dc} = \pi V_{dc}/V_\pi$ and $\phi_{dc,c} = \pi V_{dc,\,c}/V_\pi = \pi/2$. In these expressions $V_{dc}$ is the DC voltage applied to the modulator ports and $V_\pi$ is the voltage required to achieve a half wave phase shift. The input in-phase RF signal is composed of two voltage tones with equal amplitudes $V_{rf,i}$ ($\phi_{rf,i} = \pi V_{rf,i}/V_\pi$) placed at angular frequencies $\Omega_1$ and $\Omega_2$, while the quadrature RF signal is also composed of two tones with equal amplitudes $V_{rf,q}$ ($\phi_{rf,q} = \pi V_{rf,q}/V_\pi$) again placed at angular frequencies $\Omega_1$ and $\Omega_2$. After a lengthy but straightforward process, we arrive

Optics EXPRESS

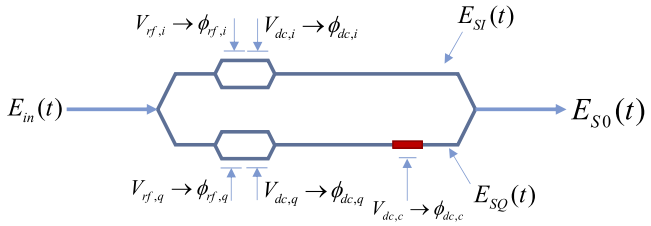


**Fig. 2.** Internal layout and signals (voltage and associated phase shift) in the Dual Parallel Mach-Zehnder Modulator considered in this work for I-Q modulation. Each arm contains an independent Mach Zehnder modulator and the lower arm includes an additional phase shift stage to provide the required π/2 delay between the in-phase and quadrature components.

at the following expression for the output field from the I-Q modulator.

$$E_{s0}(t) = \frac{j}{2}\sqrt{P_{in}\alpha_{DPMZM}}e^{j\omega_0 t} \times \left[\sum_{n=-\infty}^{\infty}\sum_{m=-\infty}^{\infty} B_{n,m}\left\{J_n\left(\frac{\phi_{rf,i}}{2}\right)J_m\left(\frac{\phi_{rf,i}}{2}\right) + jJ_n\left(\frac{\phi_{rf,q}}{2}\right)J_m\left(\frac{\phi_{rf,q}}{2}\right)\right\}e^{j(n\Omega_1+m\Omega_2)t}\right] \quad (2)$$

where $\alpha_{DPMZM}$ represents the insertion losses of the modulator, $J_n(x)$ the nth order Bessel function of the first kind, $j = \sqrt{-1}$ and the Fourier coefficients $B_{n,m}$ are given by:

$$B_{n,m,i(q)} = \left\{\frac{e^{j\frac{\phi_{dc}}{2}} - (-1)^{m+n}e^{-j\frac{\phi_{dc}}{2}}}{2j}\right\} = \begin{cases} \sin\left(\frac{\phi_{dc}}{2}\right) & m+n \text{ even} \\ -j\cos\left(\frac{\phi_{dc}}{2}\right) & m+n \text{ odd} \end{cases} \quad (3)$$

### 2.1.3. Arbitrary amplifier-filter chain

The internal configuration of this block is shown in Fig. 3. Each stage "i" is composed of an optical amplifier given by a power gain $G_i$ and an amplified spontaneous emission (ASE) noise photon number $N_i = n_{spi}(G_i\text{-}1)$, where $n_{spi}$ represents the population inversion of the amplifier. The second element of the block is an arbitrary filter given by its complex-valued optical field transfer function $H_i(\omega)$.

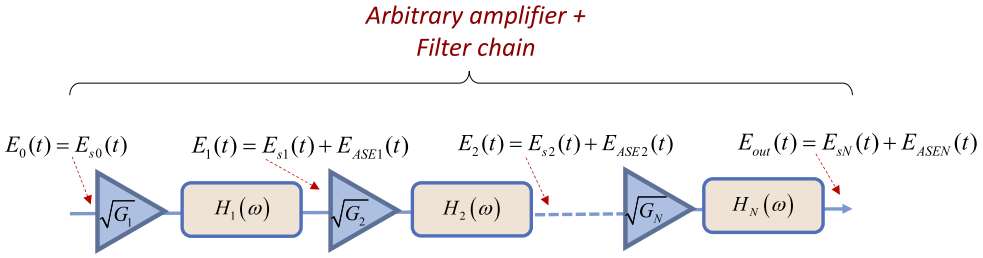


**Fig. 3.** Internal configuration of the arbitrary amplifier plus filter chain. It is composed of N amplifier plus filter stages, which can individually different.

Note that the input signal to each stage "i" is the field $E_{i-1}(t)$, which is composed of a signal part, that is the result of the input signal amplified and filtered by the i-1 previous stages and a noise component that is due to the ASE noise generated and filtered by stage "i-1" and the amplified and filtered cumulative ASE noise generated by stages "1", "2"…"i-2". The only exception is $E_0(t)$ that contains no ASE noise component. The output field from the amplifier filtered chain is labelled as $E_{out}(t)$.

Optics EXPRESS

#### 2.1.4. Local oscillator

The local CW oscillator is placed at one of the 2 inputs of the balanced detection stage. Its purpose is to beat with $E_{out}(t)$ providing an RF up-converted signal at the overall system output. The local oscillator provides an input optical field to the balanced detector given by:

$$E_{lo}(t) = \sqrt{P_{lo}} e^{(j\omega_{lo}t)} \tag{4}$$

where $P_{lo}$ is optical power and $\omega_{lo}$ the emited optical frequency. We define the difference between both optical carrier frequency as intermediate optical frequency ($|\omega_o - \omega_{lo}| = \omega_{if}$), which represent the value by which the detected RF signal is up-scaled or down-scaled.

#### 2.1.5. Balanced detection stage

Finally, the balanced detection stage is composed by a 3 dB (i.e. k = 1/2) 2 × 2 coupler that mixes $E_{out}(t)$ and $E_{lo}(t)$ yielding their sum and difference at its outputs. A pair of identical and equal responsivity photodetectors detect them respectively and their photocurrents subtracted. In this way, all common mode currents are supressed to produce the output beating current $I_{out}(t)$:

$$I_{out}(t) = j\Re\{[E_{lo}E_{sN}^{*} - E_{lo}^{*}E_{sN}] + [E_{lo}E_{ASEN}^{*} - E_{lo}^{*}E_{ASEN}]\} \tag{5}$$

where $\Re$ represents the photodetector responsivity and * denotes the complex conjugate.

### 2.2. Signal and noise sources

#### 2.2.1. Linear signal

Using the models described in section 2.1 for the different system blocks, assuming small-signal approximation and following a similar procedure to that reported in [9] we obtain the following values for the in-phase and quadrature photocurrents corresponding to the linear output produced in response to an input sinusoidal current at $\Omega_1$,:

$$I_{out,i(q)}(\Omega_1, t) \approx \Re\sqrt{P_{in}P_{lo}G\alpha_{DPMZM}}\left(\frac{\phi_{rf,i(q)}}{4}\right)\cos\left(\frac{\phi_{dc}}{2}\right)|H(\omega_o + \Omega_1)|\sin[(\omega_{if} + \Omega_1)t + \vartheta_H] \tag{6}$$

where:

$$\begin{aligned} G &= \prod_{k=1}^{N} G_k \\ H(\omega) &= \prod_{k=1}^{N} H_k(\omega) \end{aligned} \tag{7}$$

$H(\omega)$ represents the overall system transfer function (including losses) and $\theta_H$ is a phase factor.

From (6)– (7), it is straightforward to compute the corresponding RF power offered to a load resistor $R_{out}$:

$$\begin{aligned} P_{RF(out),i(q)}(\Omega_1) &= \frac{1}{T}\int_0^T I_{out,i(q)}^2(\Omega_1)R_{out}dt \\ &= \frac{\Re^2 R_{out}P_{in}P_{lo}G\alpha_{DPMZM}\phi_{rf,i}^2|H(\omega_o + \Omega_1)|^2}{32}\cos^2\left(\frac{\phi_{dc}}{2}\right) \end{aligned} \tag{8}$$

#### 2.2.2. Nonlinear signal beating terms

Using the same procedure, we can obtain the in-phase and quadrature components of nonlinear second and third-order beating photocurrents in response to an input sinusoidal current composed

Optics EXPRESS

of one tone at $\Omega_1$ and another at $\Omega_2$.

$$\begin{aligned} &I_{out,i(q)}(\Omega_1-\Omega_2,t)\approx \\ &\approx -\Re\sqrt{P_{in}P_{lo}\alpha_{DPMZM}G}\left(\frac{\phi_{rf,i(q)}}{4}\right)^2\sin\left(\frac{\phi_{dc}}{2}\right)|H(\omega_o+\Omega_1-\Omega_2)|\cos[(\omega_{if}+\Omega_1-\Omega_2)t+\vartheta_H] \\ &I_{out,i(q)}(2\Omega_1-\Omega_2,t)\approx \\ &\approx -\Re\frac{\sqrt{P_{in}P_{lo}\alpha_{DPMZM}G}}{2}\left(\frac{\phi_{rf,i(q)}}{4}\right)^3\cos\left(\frac{\phi_{dc}}{2}\right)|H(\omega_o+2\Omega_1-\Omega_2)|\sin[(\omega_{if}+2\Omega_1-\Omega_2)t+\vartheta_H] \end{aligned} \tag{9}$$

It is also convenient to compute the corresponding RF powers offered to a load resistor $R_{out}$:

$$\begin{aligned} P_{RF\_2,i(q)}(\Omega_1-\Omega_2) &= \frac{1}{T}\int_0^T I^2_{out,i(q)}(\Omega_1-\Omega_2,t)R_{out}dt \\ &= \frac{\Re^2 P_{in}P_{lo}\alpha_{DPMZM}GR_{out}}{2}\left(\frac{\phi_{rf,i(q)}}{4}\right)^4\sin^2\left(\frac{\phi_{dc}}{2}\right)|H(\omega_o+\Omega_1-\Omega_2)|^2 \\ P_{RF\_3,i(q)}(2\Omega_1-\Omega_2) &= \frac{1}{T}\int_0^T I^2_{out,i(q)}(2\Omega_1-\Omega_2,t)R_{out}dt \\ &= \Re^2\frac{P_{in}P_{lo}\alpha_{DPMZM}GR_{out}}{8}\left(\frac{\phi_{rf,i(q)}}{4}\right)^6\cos^2\left(\frac{\phi_{dc}}{2}\right)|H(\omega_o+2\Omega_1-\Omega_2)|^2 \end{aligned} \tag{10}$$

### 2.2.3. Amplified spontaneous emission noise

ASE noise is a fundamental source of degradation in amplified systems. To model the electric field corresponding to a given amplifier we employ the spectral-bin technique proposed by Desurvire [12]. The noise spectrum is then given by the sum of contributions corresponding to 2M+1 adjacent spectral bands of width δω. For amplifier 1 this model gives:

$$E_{ASE1}(t)=\sqrt{\hbar\omega_o\delta\omega}\sum_{k=-M}^{M}\sqrt{N_1}H_1(\omega_o+k\delta\omega)e^{j[(\omega_o+k\delta\omega)t+\varphi_{1,k}]} \tag{11}$$

where $\hbar$ is the Planck angular constant and $\varphi_{1,k}$ represent independent random phases. For amplifier 2, the overall ASE noise field is composed of its own generated and filtered spontaneous amplified emission plus the amplified and filtered incoming ASE from the first amplifier. Thus:

$$\begin{aligned} E_{ASE2}(t)=\sqrt{\hbar\omega_o\delta\omega}\sum_{k=-M}^{M}\Big[&\sqrt{N_1G_2}H_1(\omega_o+k\delta\omega)H_2(\omega_o+k\delta\omega)e^{j\varphi_{1,k}} \\ &+\sqrt{N_2}H_2(\omega_o+k\delta\omega)e^{j\varphi_{2,k}}\Big]e^{j[(\omega_o+k\delta\omega)t]} \end{aligned} \tag{12}$$

A similar argument runs for subsequent stages so for amplifier N, the overall ASE noise field is given by:

$$\begin{aligned} E_{ASEN}(t)&=\sqrt{\hbar\omega_o\delta\omega}\sum_{k=-M}^{M}H_{FANC}(\omega_o+k\delta\omega)e^{j[(\omega_o+k\delta\omega)t]} \\ H_{FANC}(\omega_o+k\delta\omega)&=H(\omega_o+k\delta\omega)H_{ASE}(\omega_o+k\delta\omega) \\ H_{ASE}(\omega_o+k\delta\omega)&=\sqrt{G}\left[\begin{array}{l}\dfrac{\sqrt{N_1}e^{j\varphi_{1,k}}}{\sqrt{G_1}}+\dfrac{\sqrt{N_2}e^{j\varphi_{2,k}}}{\sqrt{G_1G_2}H_1(\omega_o+k\delta\omega)}+ \\ +\dfrac{\sqrt{N_3}e^{j\varphi_{3,k}}}{\sqrt{G_1G_2G_3}H_1(\omega_o+k\delta\omega)H_2(\omega_o+k\delta\omega)}+\cdots+\dfrac{\sqrt{N_N}e^{j\varphi_{N,k}}}{\sqrt{G}\prod_{k=1}^{N-1}H_k(\omega_o+k\delta\omega)}\end{array}\right] \end{aligned} \tag{13}$$

Optics EXPRESS

ASE leads to several noise contributions after detection. In direct detection system both the signal-ASE and the ASE-ASE beat noise sources are dominant, but for balanced heterodyne detection these are in fact cancelled, leaving the ASE-local oscillator beat noise as the relevant contribution. The ASE-lo noise field is given by:

$$\begin{aligned} I_{ASE-lo}(t) &= j\Re[E_{lo}E^*_{ASEN} - E^*_{lo}E_{ASEN}] \\ &= 2\Re\sqrt{\hbar\omega_o\delta\omega P_{lo}}\sum_{k=-M}^{M}|H_{FANC}(\omega_o + k\delta\omega)|\sin[(\omega_{if} + k\delta\omega)t + \vartheta_{H_{FANC,k}}] \end{aligned} \tag{14}$$

It is straightforward to verify that:

$$\begin{aligned} \langle I_{ASE-lo}(t)\rangle &= 0 \\ \left\langle I^2_{ASE-lo}(t)\right\rangle &= 2\Re^2 R_{out}\hbar\omega_o P_{lo}|H(\omega_o)|^2 N_{eq}(\omega_o)B_{o,eq} \end{aligned} \tag{15}$$

where $B_{o,eq}$ is the equivalent optical bandwidth of the arbitrary filter and amplifier chain and $N_{eq}(\omega)$ its equivalent ASE photon number parameter:

$$\begin{aligned} N_{eq}(\omega) = G\Bigg[\frac{N_1}{G_1} + \frac{N_2}{G_1G_2|H_1(\omega_o + k\delta\omega)|^2} + \frac{N_3}{G_1G_2G_3|H_1(\omega_o + k\delta\omega)H_2(\omega_o + k\delta\omega)|^2} \\ + \cdots\frac{N_N}{G\prod_{k=1}^{N-1}|H_k(\omega_o + k\delta\omega)|^2}\Bigg] \end{aligned} \tag{16}$$

Using (14)– (16), one gets:

$$\begin{aligned} \sigma^2_{ASE-lo} &= \left\langle I^2_{ASE-lo}(t)\right\rangle - \left\langle I_{ASE-lo}(t)\right\rangle = 2\eta^2 I_N I_{lo} R_{out}|H(\omega_o)|^2 \\ I_N &= eN_{eq}(\omega_o)B_{o,eq} \\ I_{lo} &= (e/\hbar\omega_o)P_{lo} \end{aligned} \tag{17}$$

where η is the detector quantum efficiency and e is the electron charge. From (17) we finally obtain the noise spectral density and its corresponding power over an electric bandwidth $B_e$.

$$\begin{aligned} N_{ASE-lo}(f) &= \frac{4\eta^2 I_N I_{lo} R_{out}|H(\omega_o)|^2}{B_{o,eq}} \\ N_{ASE-lo} &= \frac{4\eta^2 I_N I_{lo} R_{out}|H(\omega_o)|^2 B_e}{B_{o,eq}} \end{aligned} \tag{18}$$

#### 2.2.4. Shot noise sources

There are three main shot noise sources due to the signal, local oscillator and ASE. For the shot-signal noise we have:

$$N_{shot-signal}(f) = 2e(I_{DCs,up} + I_{DCs,down})R_{out} \tag{19}$$

where $I_{DC,up(down)}$ represent the direct currents due to the signal in the upper and lower branches of the balanced detector. The optical field DC component at the output of the optical system is

Optics EXPRESS

given by:

$$E_{sN,DC}(t) = \frac{j}{2}\sqrt{P_{in}\alpha_{DPMZM}G}e^{j\omega_0 t}\sin\left(\frac{\phi_{dc}}{2}\right)(1+j)H(\omega_o) \tag{20}$$

From (20):

$$I_{DCs,up} = I_{DCs,down} = \Re\left\langle\frac{|E_{sN,DC}(t)|^2}{2}\right\rangle = \frac{\Re P_{in}\alpha_{DPMZM}G}{4}\sin^2\left(\frac{\phi_{dc}}{2}\right)|H(\omega_o)|^2 \tag{21}$$

So the noise spectral density and its corresponding power over an electric bandwidth $B_e$ for the shot-signal noise are given by:

$$\begin{aligned} N_{shot-signal}(f) &= e\eta I_S G\alpha_{DPMZM}\sin^2\left(\frac{\phi_{dc}}{2}\right)|H(\omega_o)|^2 R_{out} \\ N_{shot-signal} &= e\eta I_S G\alpha_{DPMZM}\sin^2\left(\frac{\phi_{dc}}{2}\right)|H(\omega_o)|^2 R_{out}B_e \\ I_S &= eP_{in}/\hbar\omega_o \end{aligned} \tag{22}$$

Using similar arguments and recalling the lo field given by (4), we get the noise spectral density and its corresponding power over an electric bandwidth $B_e$ for the local oscillator shot noise:

$$\begin{aligned} N_{shot-lo}(f) &= 2e\eta I_{lo}R_{out} \\ N_{shot-lo} &= 2e\eta I_{lo}R_{out}B_e \\ I_{lo} &= eP_{lo}/\hbar\omega_o \end{aligned} \tag{23}$$

Finally, using (13) we get the noise spectral density and its corresponding power over an electric bandwidth $B_e$ for the ASE shot noise:

$$\begin{aligned} N_{ASE-shot}(f) &= 2e\eta I_N M_{sp}|H(\omega_o)|^2 R_{out} \\ N_{ASE-shot} &= 2e\eta I_N M_{sp}|H(\omega_o)|^2 R_{out}B_e \end{aligned} \tag{24}$$

where $M_{sp}$ is a phenomenological parameter that accounts for the number of states of polarization in the ASE noise. $M_{sp} = 1$ for semiconductor amplifiers and $M_{sp} = 2$ for fiber amplifiers in general.

#### 2.2.5. Total noise

Due to the use of a balanced detection configuration, all common mode noise sources usually present in direct detection systems are cancelled or greatly suppressed here. This accounts for the input thermal noise, the RIN noise and, as mentioned before, the signal-ASE and ASE-ASE beating noises. Therefore, the overall noise is given by the contributions discussed in 2.2.3 and 2.2.4 together with the output thermal noise:

$$\begin{aligned} N_T(f) &= \frac{4\eta^2 I_N I_{lo}R_{out}|H(\omega_o)|^2}{B_{eq,o}} + e\eta I_S G\alpha_{DPMZM}\sin^2\left(\frac{\phi_{dc}}{2}\right)|H(\omega_o)|^2 R_{out} \\ &\quad + 2e\eta I_{lo}R_{out} + 2e\eta I_N M_{sp}|H(\omega_o)|^2 R_{out} + k_B T \\ N_T &= \left[\frac{4\eta^2 I_N I_{lo}R_{out}|H(\omega_o)|^2}{B_{eq,o}} + e\eta I_S G\alpha_{DPMZM}\sin^2\left(\frac{\phi_{dc}}{2}\right)|H(\omega_o)|^2 R_{out}\right. \\ &\quad \left. + 2e\eta I_{lo}R_{out} + 2e\eta I_N M_{sp}|H(\omega_o)|^2 R_{out} + k_B T\right] B_e \end{aligned} \tag{25}$$

## 3. Figures of merit

We now use the results derived in section 2 to find the expressions for the typical FOMs of a microwave photonics system.

Optics EXPRESS

### 3.1. RF gain

We define the RF Gain as the ratio between the input RF power ($P_{RFin}(\Omega)$) and the output RF photodetected power ($P_{RFout}(\Omega)$). Using (8) and taking $P_{RFin,i(q)}(\Omega) = V_{rf,i(q)}{}^2/(2R_{in})$:

$$G_{RF,i(q)}(\Omega_1) = \frac{\eta^2 R_{out} R_{in} I_s I_{lo} \pi^2 G \alpha_{DPMZM} |H(\omega_o + \Omega_1)|^2}{8V_\pi^2} \cos^2\left(\frac{\phi_{dc}}{2}\right) \tag{26}$$

Note that the RF gain is identical for both the in-phase and quadrature components.

### 3.2. Noise figure

The noise figure of the MWP link is [13]:

$$NF = \frac{N_T}{G_{RF} k_B T} \tag{27}$$

And is given by substituting (25) and (26) into (27).

### 3.3. Dynamic range

Finally, the link dynamic range can be evaluated through the second and third order Spurious Free Dynamic Ranges (SFDR). These are given in terms of the second and third-order output intercept points respectively ($OIP_2$ and $OIP_3$) [13]:

$$\begin{aligned} SFDR_2 &= \left[\frac{OIP_2}{N_T}\right]^{1/2} \\ SFDR_3 &= \left[\frac{OIP_3}{N_T}\right]^{2/3} \end{aligned} \tag{28}$$

To compute OIP2 and OIP3 we equal Eq. (8) to those on Eq. (10):

$$\begin{aligned} OIP2|_{\Omega_1-\Omega_2,i(q)} &= \frac{\Re^2 R_{out} P_{in} P_{lo} G \alpha_{DPMZM} |H(\omega_o + \Omega_1)|^4}{4|H(\omega_o + \Omega_1 - \Omega_2)|^2} \cdot \frac{[1+\cos\phi_{dc}]^2}{[1-\cos\phi_{dc}]} \\ OIP3|_{2\Omega_1-\Omega_2,i(q)} &= \frac{\Re^2 R_{out} P_{in} P_{lo} G \alpha_{DPMZM} |H(\omega_o + \Omega_1)|^3 [1+\cos\phi_{dc}]}{2|H(\omega_o + 2\Omega_1 - \Omega_2)|} \end{aligned} \tag{29}$$

This completes the derivation of the main FOMs.

## 4. Discussion, applications and results

### 4.1. Discussion

Equations (6)–(29) describe de model and main figures of merit as a function of the system's relevant transmission parameters. Note that the RF gain is not governed by the squared value of the optical gain as in direct detection systems [9]. In this approach the RF gain is governed by the product of the overall optical gain of the link and the local oscillator power, which enables the adjustment of the RF gain by tuning the power of the latter. This feature is expected as the useful signal current is linearly related to the link optical field and not the power. Observe that the optical segment has been modelled using cells where the optical amplification precedes the filtering, however, it also accounts for the case where it is the amplifier that follows the filter. In this case, one needs only to make $G_1 = 1$. Note as well again that several noise sources are not present in (25), which are relevant in direct detection systems. For instance, the laser relative intensity noise (RIN), the spontaneous-spontaneous and signal-spontaneous beat noises

Optics EXPRESS

are cancelled by the balanced detector. It is also worth noticing that Eq. (16), which is central in the model and plays a similar role to the Friis formula in direct detection systems.

The model is very general and accounts for MWP systems with arbitrary complexity, provided that the optical segment filtering and amplification is linear. This is the common situation in practice, where optical amplifiers are employed for signal loss mitigation and therefore no gain saturation is expected. Note that this is the case of both, integrated MWP links and discrete components based links. It is probable that for MWP complex systems may include up to two or three filtering stages and perhaps two to three amplifiers. For these cases, our model can be readily specialised. In addition, the analytic nature of our results allows for very fast simulation and its multi-parameter nature tolerates for the fast evaluation of 2-dimensional performance maps leaving the rest of the parameters *ceteris paribus*.

### 4.2. Application example

The model can be applied to MWP systems featuring considerable complexity regardless of whether the final application is focused on transmission (radio over fiber systems, 5G front-haul links. . . etc.) or signal processing (i.e. filtering, true-time delaying, up-conversion, beamforming. . . etc.). Here, we consider an example that is representative of a Central Office (CO) to Base-Station (BS) front-haul link in a 5G communications system as shown in Fig. 4. Coherent detection is employed at the BS for signal up-conversion.

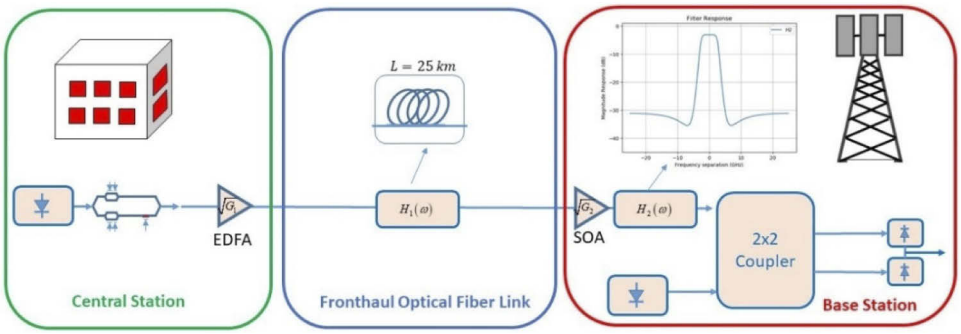


**Fig. 4.** Coherent heterodyne MWP system representing a Central Office to Base Station 5G front-haul link with up-conversion.

In this case, the I-Q modulator and an Erbium-Doped Fiber Amplifier (EDFA) are assumed as part of the CS equipment. The front-haul connection is implemented by means of a 25Km optical fiber link and the BS equipment includes an online signal processing stage implemented by a photonic chip composed of a semiconductor optical amplifier (SOA) and an optical elliptic filter, followed by the heterodyne balanced detection stage. Overall, the link is composed of two amplifier and filter stages.

The model can be employed to analyze the end-to-end system performance and moreover, to investigate the effect that the variation of one or more parameters can have on the overall figures of merit. To this aim, we have considered three examples that represent different design options for the system in Fig. 4. Example 1, represents a design where amplifiers are employed to compensate for losses and low power lasers are employed both for the CS source and the local oscillator. Example 2, illustrates the case where the local oscillator laser power is increased to boost the detected RF signal and example 3 corresponds to the case where the detected RF signal power is increased by the combined effect of a higher EDFA gain and moderate local oscillator power. The values of the main system parameters in each example are shown in Table 1.

Optics EXPRESS

**Table 1. Main system parameters of three representative design alternatives for the front-haul link of Fig. 4.**

| Parameters set to perform the simulation | Example 1 | Example 2 | Example 3 |
|---|---|---|---|
| $f_1$ | 1GHz | 1GHz | 1GHz |
| $f_2$ | 1.2GHz | 1.2GHz | 1.2GHz |
| $\mathbf{P_{in}}$ | 0dBm | 0dBm | 0dBm |
| $\mathbf{P_{LO}}$ | 0dBm | 13dBm | 5dBm |
| $\mathbf{G_{EDFA}}$ | 13dB | 13dB | 25dB |
| $\mathbf{NF_{EDFA}}$ | 4dB | 4dB | 4dB |
| $\mathbf{G_{SOA}}$ | 9dB | 9dB | 9dB |
| $\mathbf{NF_{SOA}}$ | 6dB | 6dB | 6dB |
| $\boldsymbol{\alpha_{mzm}}$ | 4dB | 4dB | 4dB |

The model renders the values for the main figures of merit of each example according to Eqs. (26)–(29) with the proper parameter value substitution. It also provides useful information that can be visually represented in Fig. 5. Then, Table 2 show the results corresponding to the noise sources for each of the three examples. This allows, for example, to identify if there is a dominant noise source or if on the contrary, two or more sources need to be taken into account. For instance, and in the considered application scenario, we can observe that shot-signal noise dominates in example 1, while LO driven noise is the predominant noise in the other two cases.

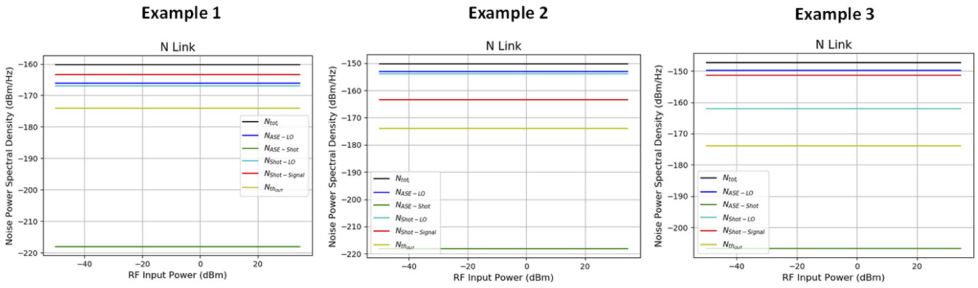


**Fig. 5.** Noise densities of different sources for the three examples considered in Table 1.

**Table 2. Numeric values of noise densities of different sources for the three examples considered in Table 1.**

| Noise densities | Example 1 | Example 2 | Example 3 |
|---|---|---|---|
| $\mathbf{N_{\mathit{shot-signal}}}$ | -163.40dBm/Hz | -163.40dBm/Hz | -151.40dBm/Hz |
| $\mathbf{N_{\mathit{ase-lo}}}$ | -166.11dBm/Hz | -153.11dBm/Hz | -149.75dBm/Hz |
| $\mathbf{N_{\mathit{shot-lo}}}$ | -166.98dBm/Hz | -153.98dBm/Hz | -161.99dBm/Hz |
| $\mathbf{N_{\mathit{th-out}}}$ | -173.98dBm/Hz | -173.98dBm/Hz | -173.98dBm/Hz |
| $\mathbf{N_{\mathit{ase-shot}}}$ | -218.04dBm/Hz | -218.04dBm/Hz | -206.68dBm/Hz |
| $\mathbf{N_{\mathit{tot}}}$ | -160.26dBm/Hz | -150.28dBm/Hz | -147.32dBm/Hz |

Indeed, the fact that the end-to-end model provides an estimation of the rest of the FOMs, allows us to dispose of the complete information upon which to decide which is the best design option. Table 3 shows, in form of a comparative table, the results obtained for the main figures

Optics EXPRESS

of merit in each of the three design examples. Overall, as it can be appreciated, example 3 provides the best alternative as far as RF Gain is concerned (17dB increase) providing also a 2.7dB improvement in dynamic range (SFDR3).

**Table 3. Overall Figures of merit for the application examples described in Table 1.**

| | MWP Power-Amplified Link Example 1 | MWP Power-Amplified Link Example 2 | MWP Power-Amplified Link Example 3 |
|---|---|---|---|
| **Gain Link** | -29.96dB | -16.96 dB | -12.96 dB |
| **NF Link** | 43.67dB | 40.65 dB | 39.61 dB |
| **Noise Spectral Density** | -160.26dBm/Hz | -150.28 dBm/Hz | -147.32 dBm/Hz |
| **SFDR2** | 75.05dBm/Hz$^{1/2}$ | 76.56 dBm/Hz$^{1/2}$ | 77.08 dBm/Hz$^{1/2}$ |
| **SFDR3** | 101.67 dBm/Hz$^{2/3}$ | 103.69 dBm/Hz$^{2/3}$ | 104.38 dBm/Hz$^{2/3}$ |

## 5. Conclusion

We have reported an end-to-end analytic model for the computation of the FOMs of arbitrarily filtered and amplified heterodyne coherent MWP links. It is useful for evaluating the performance of complex systems where the final stage is employed for up/down converting the RF signal. We have applied the model to a specific case of complex system representing the front-haul segment in a 5G link between the central office and the base station. Three different scenarios that trade-off amplifier gain and local oscillator power have been considered, showing that the model can anticipate the expected performance of each design alternative. The model can be applied to a wider range of cases combining fiber and photonic chip elements and thus is expected to provide a useful and fast tool to analyze them in the design stage.

**Funding.** Huawei Technologies (YBN202006512); European Research Council (ADG-2016 UMWP-Chip); Generalitat Valenciana (PROMETEO 2021/015).

**Acknowledgments.** The authors wish to acknowledge Huawei for the funding of this research through Research & development agreement YBN202006512. E.S, D.P, and J.C acknowledge support by the ERC ADG-2016 UMWP-Chip, the Generalitat Valenciana PROMETEO 2021/015 research excellence award.

**Disclosures.** The authors declare no conflicts of interest.

**Data availability.** No additional data were generated or analyzed in the presented research. All relevant data in the present research are included in the paper.

## References

1. J. Yao, "Microwave photonics," J. Lightwave Technol. **27**(3), 314–335 (2009).
2. J. Capmany and D. Novak, "Microwave photonics combines two worlds," Nature Photon **1**(6), 319–330 (2007).
3. D. Marpaung, J. Yao, and J. Capmany, "Integrated microwave Photonics," Nat. Photonics **13**(2), 80–90 (2019).
4. I. Gasulla and J. Capmany, "Analytical model and figures of merit for filtered microwave photonic links," Opt. Express **19**(20), 19758–19774 (2011).
5. V. J. Urick, K.J. Williams, and J. D. McKinney, *Fundamentals of microwave photonics,* (John Wiley & Sons, 2015).
6. Y. Liu, D. Marpaung, A. Choudhary, J. Hotten, and B. J. Eggleton, "Link performance optimization of chip-based Si3N4 microwave photonic filters," J. Lightwave Technol. **36**(19), 4361–4370 (2018).
7. D. Pérez, I. Gasulla, J. Capmany, J. S. Fandiño, P. Muñoz, and H. Alavi, "Figures of merit for self-beating filtered microwave photonic systems," Opt. Express **24**(9), 10087–10102 (2016).
8. V. J. Urick, M. E. Godinez, P. S. Devgan, J. D. McKinney, and F. Bucholtz, "Analysis of an analog fiber-optic link employing a low-biased Mach–Zehnder modulator followed by an erbium-doped fiber amplifier," J. Lightwave Technol. **27**(12), 2013–2019 (2009).
9. E. Sánchez, D. Pérez-López, P. dasMahapatra, and J. Capmany, "Modeling amplified arbitrary filtered microwave photonic links and systems," Opt. Express **29**(10), 14757–14772 (2021).
10. C.G. Bottenfield, V.A. Thomas, and S.E. Ralph, "Analytic Equations for Photonic Frequency Converter Design," J. Lightwave Technol. **39**(24), 7706–7715 (2021).
11. T. Nakasyotani, H. Toda, T. Kuri, and K. Kitayama, "Wavelength-division-multiplexed Millimeterwaveband radio-on-fiber system using a supercontinuum light source," J. Lightwave Technol. **24**(1), 404–410 (2006).

Optics EXPRESS

12. E. Desurvire, *Erbium Doped Fiber Amplifiers* (John Wiley & Sons, 1994).
13. C. H. Cox III, *Analog Photonic Links: Theory and Practice*. (Cambridge University, 2004).